

Frequency and Angular Variations of Land Surface Microwave Emissivities: Can We Estimate SSM/T and AMSU Emissivities from SSM/I Emissivities?

Catherine Prigent, Jean-Pierre Wigneron, *Member, IEEE*, William B. Rossow, and Juan R. Pardo-Carrion

Abstract—To retrieve temperature and humidity profiles from special sensor microwave/temperature (SSM/T) and advanced microwave sounding units (AMSU), it is important to quantify the contribution of the Earth surface emission. So far, no global estimates of the land surface emissivities are available at SSM/T and AMSU frequencies and scanning conditions. The land surface emissivities have been previously calculated for the globe from the SSM/I conical scanner between 19 and 85 GHz. To analyze the feasibility of deriving SSM/T and AMSU land surface emissivities from SSM/I emissivities, the spectral and angular variations of the emissivities are studied, with the help of ground-based measurements, models, and satellite estimates. Up to 100 GHz, for snow and ice free areas, the SSM/T and AMSU emissivities can be derived with useful accuracy from the SSM/I emissivities. The emissivities can be linearly interpolated in frequency. Based on ground-based emissivity measurements of various surface types, a simple model is proposed to estimate SSM/T and AMSU emissivities for all zenith angles knowing only the emissivities for the vertical and horizontal polarizations at 53° zenith angle. The method is tested on the SSM/T-2 91.655 GHz channels. The mean difference between the SSM/T-2 and SSM/I-derived emissivities is ≤ 0.01 for all zenith angles with a root mean squared (RMS) difference of ≈ 0.02 . Above 100 GHz, preliminary results are presented at 150 GHz based on SSM/T-2 observations and are compared with the very few estimations available in the literature.

Index Terms—ATOVS, microwave radiometry, surface emissivity.

I. INTRODUCTION

THE special sensor microwave/temperature 1 and 2 (SSM/T-1 and -2) and the advanced microwave sounding units A and B (AMSU-A and -B) are both cross-track temperature and water vapor profilers with similar frequencies, but AMSU has better spatial resolution. The SSM/T instruments are onboard the Defence Meteorological Satellite Program (DMSP) polar orbiting satellites. SSM/T-1 has seven channels in the O₂ absorption band around 60 GHz for temperature sounding of the atmosphere [1]. The SSM/T-2 is a water vapor profiler with five channels, three in the H₂O absorption line at 183.3 GHz and two window channels at 91.655 and 150 GHz [2]. The advanced microwave sounding unit (AMSU), part of

the advanced TIROS operational vertical sounder (ATOVS), replaces the microwave sounding unit (MSU) on the previous NOAA polar orbiters. AMSU includes a temperature sounder (AMSU-A) with 12 channels located in the O₂ absorption band around 60 GHz plus three window channels and a humidity sounder (AMSU-B) with channels centered on the water vapor absorption line at 183.3 GHz. The instruments are described in [3] and [4]. The SSM/T and AMSU instruments have cross-track scanning mechanisms, with zenith angles on the Earth up to $\sim 48^\circ$ for SSM/T and up to $\sim 58^\circ$ for AMSU. The polarization observed by SSM/T and AMSU rotates with scan angle due to the rotating-reflector/fixed-feed type of antenna design. Table I summarizes the SSM/T and AMSU characteristics and gives the total atmospheric transmission at nadir for each channel for two standard atmospheres. Channels with frequencies away from the centers of the O₂ and H₂O absorption lines not only sense emission from the troposphere, but they are also affected by the Earth surface emission. As a consequence, to retrieve atmospheric temperature and humidity profiles from the SSM/T and AMSU measurements, it is important to understand and quantify the contribution of the Earth surface emission to the observations. Using information theory, English [5] quantifies the sensitivity of the temperature and humidity retrievals to surface emissivity errors and concludes that, for temperature sounding in cloudy areas and for humidity soundings, accurate estimates of the surface emissivity and the surface skin temperature are required to use AMSU sounding data effectively.

The microwave radiative properties of the ocean have been the object of several studies in the past, from model developments, airborne measurements to satellite observations (see for instance [6]–[8]), and are now fairly well understood. Moreover, the low emissivity of the ocean in the microwave region reduces the surface radiative contributions and makes it easier to observe the atmospheric phenomena against this cold background. Land surface emissivities are not only expected to be much higher (usually close to unity), making the surface contribution larger, but they are also more variable with location and very complex to model. Efforts have been directed toward a better understanding of the mechanisms responsible for the microwave emission of soil and vegetation, from both theoretical analysis and field experiments (truck-mounted instruments [9]–[11] or airborne instruments [12]–[15]). Even assuming that a perfect land surface emissivity model exists, the number of inputs it is likely to require (soil texture and humidity, vegetation characteristics, percentage of vegetation coverage within a field

Manuscript received April 12, 1999; revised November 19, 1999.

C. Prigent, J. R. Pardo, and W. B. Rossow are with NASA Goddard Institute for Space Studies, Columbia University, New York, NY 10025 USA (e-mail: cprigent@giss.nasa.gov).

J.-P. Wigneron is with the Institut National de la Recherche Agronomique (INRA), Station de Bioclimatologie, Agroparc, Avignon, France.

Publisher Item Identifier S 0196-2892(00)06218-5.

TABLE I
SSM/T AND AMSU CHARACTERISTICS

Channel number	Frequency (GHz)	Polarization at nadir	Resolution at nadir (km)	Atmospheric transmission (tropical)	Atmospheric transmission (winter subarctic)
<i>SSM/T-1</i>					
1	50.500	H	175	.62	.67
2	53.200	H	175	.20	.22
3	54.350	H	175	.02	.02
4	54.900	H	175	.00	.00
5	58.400	V	175	.00	.00
6	58.825	V	175	.00	.00
7	59.400	V	175	.00	.00
<i>SSM/T-2</i>					
8	91.655	H	88	.60	.91
9	150.000	H	54	.23	.84
10	183.31±7.00	H	48	.00	.40
11	183.31±3.00	H	48	.00	.07
12	183.31±1.00	H	48	.00	.00
<i>AMSU-A</i>					
1	23.8	V	50	.78	.99
2	31.4	V	50	.89	.96
3	50.3	V	50	.63	.68
4	52.8	V	50	.29	.32
5	53.596±.115	H	50	.11	.13
6	54.40	H	50	.02	.02
7	54.94	V	50	.00	.00
8	55.50	H	50	.00	.00
9	57.290=ν	H	50	.00	.00
10	ν±.217	H	50	.00	.00
11	ν±.322±.048	H	50	.00	.00
12	ν±.322±.022	H	50	.00	.00
13	ν±.322±.010	H	50	.00	.00
14	ν±.322±.0045	H	50	.00	.00
15	89.0	V	50	.61	.91
<i>AMSU-B</i>					
16	89.0±.9	V	15	.61	.91
17	150.0±.9	V	15	.23	.84
18	183.31±1.00	V	15	.00	.00
19	183.31±3.00	V	15	.00	.07
20	183.31±7.00	V	15	.00	.40

of view, etc.) will not be available on a global basis with a resolution compatible with the satellite resolution.

Microwave land surface emissivities over the globe have been estimated from the special sensor microwave/imager (SSM/I) observations by removing the contributions of the atmosphere, clouds, and rain using ancillary satellite data [16], [17]. The SSM/I instrument is described in [18]. Cloud-free SSM/I observations are first isolated with the help of collocated visible/infrared satellite observations from International Satellite Cloud Climatology Project (ISCCP) data [19]. Then, the cloud-free atmospheric contribution is calculated from an estimate of the local atmospheric temperature-humidity profile from the National Centers for Environmental Prediction (NCEP) analysis [20]. Finally, with a surface skin temperature derived from IR observations (ISCCP estimate), the surface emissivity is calculated for all the SSM/I channels. The emissivities are estimated for a 53° zenith angle at 19.35, 22.235, 37.0, and 85.5 GHz for both vertical and horizontal polarizations with the exception of

22 GHz, which has vertical polarization only. The emissivities are available on a 1/4° grid, compatible with the ~30 × 30 km ISCCP DX grid and with the SSM/I observations, which are sampled at 25 km. The standard deviation of the day-to-day variations of the retrieved emissivities within a month is typically about 0.012 for all the SSM/I frequencies, which is an upper limit on uncertainty of these estimates. Biases arising from uncertainties in the IR emissivity are < 0.02 [16].

Similar techniques could be applied to SSM/T and AMSU observations to derive the land surface emissivities for each frequency and scanning angle, but because the viewing angles of SSM/T and AMSU are not constant, most scenes on the globe are not seen more than once a month under clear sky conditions with the same angle. Thus, to obtain an adequate climatology, a long time series of data (three years at least) would have to be processed before having reliable estimates of the natural variability of the surface emissivities. AMSU is now operational since January 1999, and as the data become available, calcula-

tions of the emissivities will be performed at the Centre de Météorologie Spatial, Lannion, France, with a method similar to the one developed for SSM/I. However, before an adequate time series of the emissivities becomes available, some practical alternative has to be implemented now in order to efficiently process the satellite data over land.

We examine the feasibility of estimating the SSM/T and AMSU emissivities over the globe from the previously retrieved SSM/I emissivities, taking into account the different frequencies of observation and the different scanning and polarization mechanisms of the instruments. In France at the Institut National de la Recherche Agronomique (INRA), Avignon, France, ground-based emissivity measurements have been obtained between 1.4 and 90 GHz over different surface types. Emissivity models have been derived from these measurements (Section II), and they are used to analyze the frequency and angular dependence of the surface emissivities, along with other measurements and model results available in the literature. In Section III, the emissivity variation with frequency is examined with models with results from field experiments and compared to the emissivity frequency dependence derived from the SSM/I observations. The angular and polarization variations of surface emissivities are then studied (Section IV). A simple model is proposed to derive SSM/T and AMSU land surface emissivities from SSM/I emissivities for all zenith angles and for frequencies up to 100 GHz. In Section V, the method is verified for SSM/T-2 emissivity estimates at 91.655 GHz and the extension of the method to frequencies above 100 GHz is discussed. Section VI concludes this study.

II. A MICROWAVE EMISSIVITY MODEL DERIVED FROM MEASUREMENTS UP TO 90 GHz

Simple models were calibrated on experimental data acquired over bare soils and a wheat field during the PORTOS-93 experiment in Avignon, France [10], [11]. The measurements were performed with the multifrequency microwave radiometer PORTOS (1.4, 5.05, 10.65, 23.8, 36.5 and 90 GHz) during the spring of 1993 on a plot located on the INRA Avignon Agricultural Research Center test site. Only the observations at the higher frequencies (23.8, 36.5 and 90 GHz) are considered here.

The soil is a silt-loam (27% clay, 11% sand dry weight). Three surface types are studied: a wheat field, smooth bare soil, and rough bare soil. The standard deviation of height and the horizontal correlation length characterizing the roughness conditions are 8.9 mm and 71.5 mm, respectively, for the smooth bare soil, and 19.1 mm and 65.7 mm, respectively, for the rough bare soil.

To simulate the bare soil microwave emission, a simple approach based on two best-fit roughness parameters h_S and Q_S [21] and the exponent N_S were used to fit the PORTOS observations. The p -polarized soil emissivity ϵ_{Sp} is given by

$$\epsilon_{Sp} = 1 - \left[\left(1 + \epsilon_{Sp}^{\text{spec}} (Q_S - 1) - Q_S \epsilon_{Sq}^{\text{spec}} \right) \times \exp(-h_S \cos^{N_S}(\theta)) \right] \quad (1)$$

TABLE II
SOIL PARAMETERS FOR THE INRA MODEL

Soil type	Frequency (GHz)	h_{SOIL}	Q_{SOIL}	N_{SOIL}
Smooth soil	23.8	0.43	0.23	0.0
	36.5	0.15	0.33	0.0
	90.0	0.41	0.31	0.0
Rough soil	23.8	0.57	0.43	0.5
	36.5	0.62	0.45	0.5
	90.0	0.71	0.40	0.5
Wheat field	23.8	0.40	0.37	0.0
	36.5	1.00	0.37	0.0
	90.0	0.50	0.40	0.0
		ϵ_{VEG}	α_v	α_h
	23.8	.965	0.43	0.23
	36.5	.980	0.08	1.05
	90.0	.980	0.23	0.23

where p and q stand for the vertical or horizontal polarizations, $\epsilon_{Sp}^{\text{spec}}$ is the p -polarized specular emissivity, and h_S and Q_S are, respectively, the roughness and the polarization mixing parameters. N_S is an exponent fitted to reproduce the angular variations. The soil dielectric permittivity is calculated from the model described in Calvet *et al.* [22]. The values of the average best-fit parameters h_S , Q_S and N_S are given in Table II for the three plots and the three frequencies.

To account for the effect of the vegetation canopies, the emissivity ϵ_C of a vegetated surface is computed as follows for the p -polarization:

$$\epsilon_{Cp} = \epsilon_{Sp} \times f_{Sp} + (1 - f_{Sp}) \times \epsilon_V \quad (2)$$

where ϵ_{Sp} is the emissivity of the bare soil calculated from the previous equations, ϵ_V is the emissivity of the vegetation cover, and f_{Sp} is the fraction of bare soil.

The modeling is based on several assumptions. It assumes that the vegetation emissivity simply depends on the crop type and frequency and that it does not vary with polarization or incidence angle. The variation of emissivity as a function of incidence angle and polarization for a well-developed homogeneous vegetation canopy is generally very small ([13], [16], [17]). There are very few studies in the literature that describe how the vegetation characteristics (moisture content, structure) affect these variations. For heterogeneous vegetation covers, including mixed bare soil and vegetated areas, the dependence of vegetation emissivity as a function of incidence angle and polarization can be significant (in particular for crops which are generally arranged in rows). Since crops are generally arranged in rows, geometrical effects may be significant. To account for this effect, a model is developed for polarization p

$$f_{Sp} = (1 - \alpha_p \times \tan(\theta)) \times f_{S0} \quad (3)$$

where α_p is a best-fit coefficient, and f_{S0} is the fractional coverage of soil seen at nadir. However, this last equation can be considered as a modeling refinement for crop covers with row structure and is likely to be unnecessary for large scale footprints, which include a variety of surface types.

The simple model described here for vegetation and soil provides a good fit to the available observations with an average

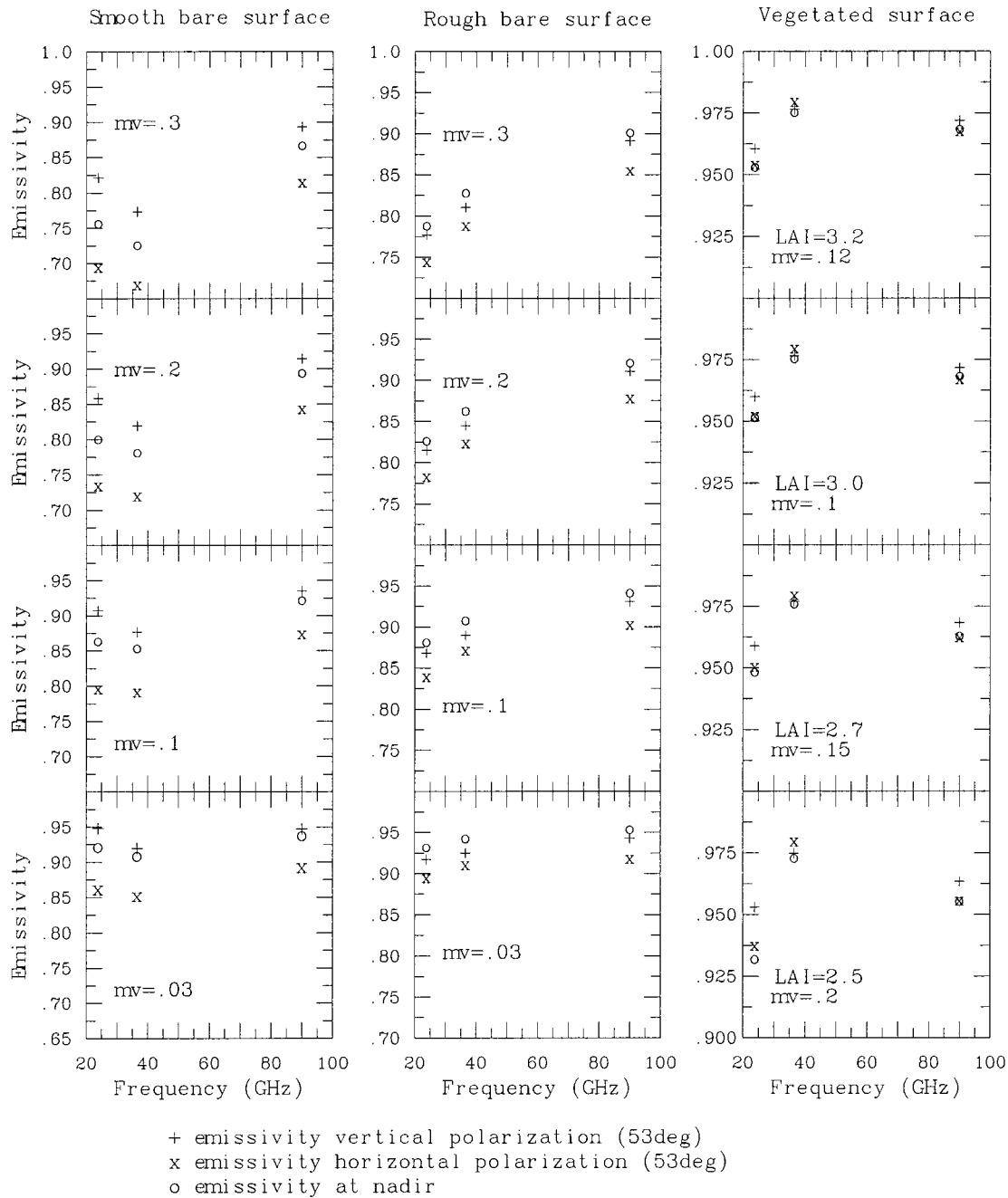


Fig. 1. Frequency dependence of land surface emissivities as measured at INRA at 23.8, 36.5, and 90 GHz. Results are presented for nadir views and for 53° incidence for smooth and rough bare surfaces with various volumetric moisture m_v and for a wheat crop at different growth stages.

RMS error of 0.002 between measured and simulated emissivities. This model is used in our study to analyze the frequency and angular dependence of the land surface emissivities up to 100 GHz.

III. THE FREQUENCY DEPENDENCE OF MICROWAVE EMISSIVITY

A. From Models and in Situ Measurements

Except for snow and ice surfaces, the frequency dependence predicted by models up to 100 GHz is gradual over a factor of ~ 5 in frequency. Fig. 1 shows the frequency dependence of the

emissivities at nadir and at 53° incidence angle for both orthogonal polarizations from the INRA measurements. Results are presented for both smooth and rough bare surfaces with varying volumetric moisture m_v , and for a wheat crop at different growth stages (indicated by the leaf area index [LAI]). Emissivities at 90 GHz are higher than at 23.8 GHz, whatever the surface type. From 36.5 to 90 GHz, the trend is less clear, with an increase or a decrease of the emissivities with frequency, depending on the surface type. Over bare soils, field measurements usually show an increase of the emissivity with increasing frequency [9], [22], [23]. The increase seems to be larger for wetter soils [22]. Over vegetated areas, the frequency dependence varies with both the

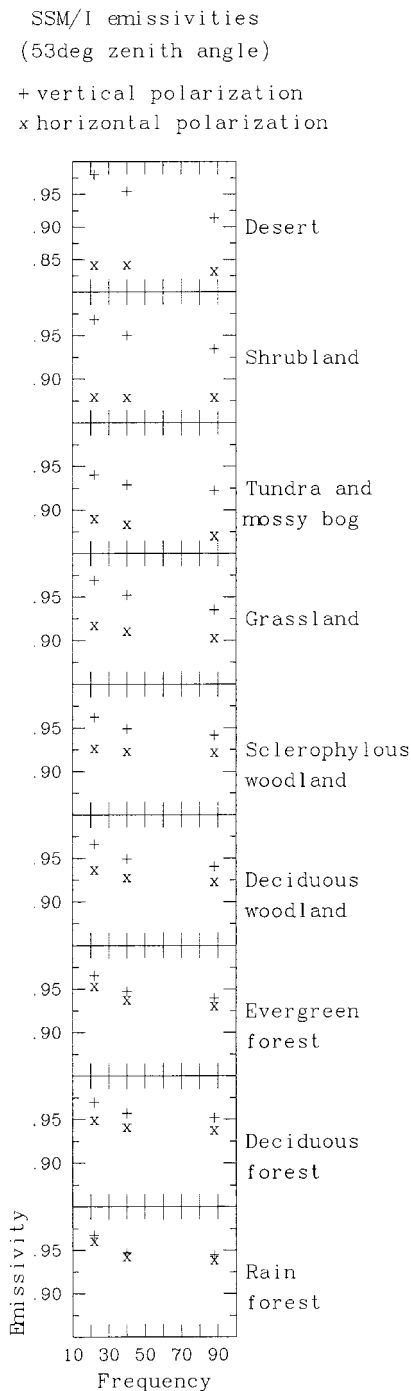


Fig. 2. Frequency dependence of the mean estimated surface emissivity for different surface types (as described by Matthews [25]). Emissivities are estimated from SSM/I at 53° zenith angle for the Meteosat area (Africa plus large portions of Europe and Western Asia) for October 1991.

vegetation characteristics and the measurement conditions (polarization and viewing angle). Over coniferous forest, Wigneron *et al.* [13] observed higher emissivities at 36.5 GHz than at 23.8 and 90 GHz. At 50° zenith angle, Matzler [23] measured a decreasing emissivity for horizontal polarization between 21 and 94 GHz and a decrease in the vertical emissivity between 21 and 35 GHz followed by an increase between 35 and 94 GHz over medium grass, while over short grass, the vertical polar-

ization emissivity increases with frequency and the horizontal polarization increases up to 35 GHz and then decreases. Over an oat field, Matzler [9] also measured decreasing or increasing emissivities depending on the phenological stage of the oat field and on the polarization. For a large variety of surface types, airborne measurements at 24, 50, 89, and 150 GHz were conducted by the U.K. Meteorological Office [14], [15]. To our knowledge, these are the only field measurements of emissivities at frequencies above 100 GHz. These observations also show different emissivity spectra, depending on the surface type. For most surface types, the emissivities at nadir increase between 24, 89, and 150 GHz. However, except for snow, ice and water surfaces, the emissivities at 50 GHz are higher than at 24 and 89 GHz. In summary, the available field measurements do often show a slight increase in emissivity with frequency, although they do not always indicate a consistent monotonic frequency dependence of surface emissivities between 20 and 150 GHz.

The RADTRAN surface model calculates vertically and horizontally polarized surface emissivities for various surface types for frequencies up to 40 GHz [24]. The modeling approach for vegetation and bare soil is based on radiative transfer theory, where the vegetation is treated as layers of continuous random media bounded by an underlying homogeneous soil layer. The RADTRAN model predicts an increase in emissivity with frequency for vegetation and for bare soil. However, the comparison between simulations and SSM/I data provided in [24] shows that the surface emissivity is somewhat overestimated by the model at 37 GHz (case c in Fig. 3 in the paper).

B. From Satellite-Based Estimates

The SSM/I frequencies range from 19 to 85 GHz. For most surfaces, the emissivities in this frequency range vary smoothly with frequency for both orthogonal polarizations at 53° incidence angle [16]. For nine vegetation classes derived from Matthews [25], Fig. 2 shows the frequency dependence of the mean surface emissivity at 53° zenith angle for each surface type, as calculated for the Meteosat area (Africa plus large portions of Europe and Western Asia) for October 1991. Whatever the vegetation type, the emissivities slowly decrease with frequency for both orthogonal polarizations. For the vertical polarization, the emissivity change between 19 and 85 GHz rarely exceeds 0.05 and is smaller over dense vegetation than over bare soil. For the horizontal polarization, the changes are smaller still (always ≤ 0.025). Under snow and ice conditions, the surface emissivity varies more quickly with frequency, and these surface types will have to be studied further.

Alternative estimates of microwave surface emissivities from satellite in this frequency range are scarce. However, all the available estimates from SSM/I observations show that, for various surfaces (bare soil, vegetated soil), the surface emissivity decreases with increasing frequency for both vertical and horizontal polarizations at 53° incidence. Choudhury [26] analyzed rain forest and desert locations for the period January 1988 to December 1989 and found that emissivities at 37 GHz are almost always lower than at 19 GHz for both orthogonal polarizations. For a 70-day period over the central United States, Jones and Vonder Haar [27] also observed a decrease in emissivity

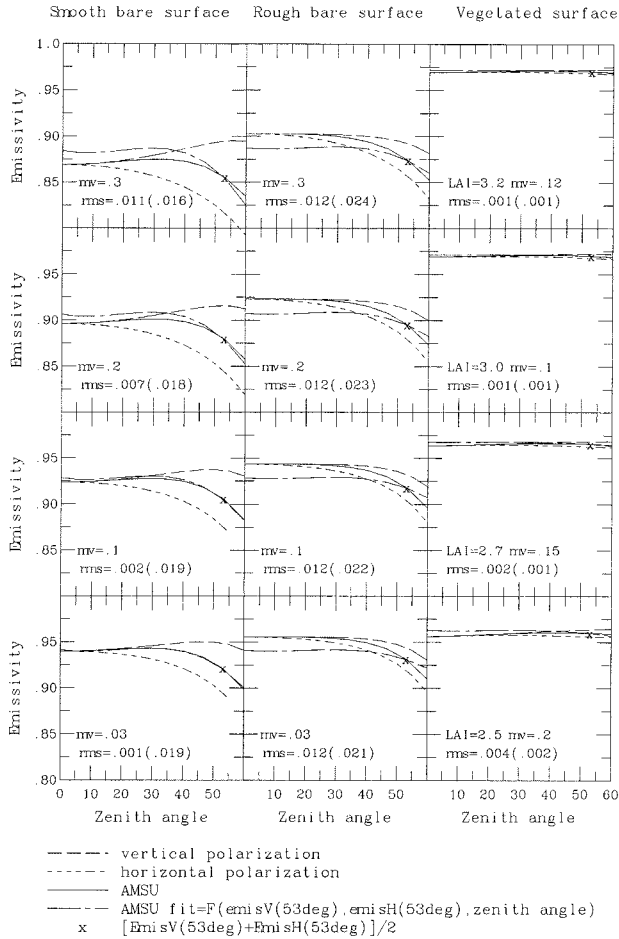


Fig. 3. Angular dependence of land surface emissivities given by the INRA models at 90 GHz. Results are presented for smooth and rough bare surfaces with various volumetric moisture m_v and for a wheat crop at different growth stages (indicated by the leaf area index [LAI]). The emissivities that would be seen with an AMSU-like instrument are indicated (solid lines), along with the best-fit function to these emissivities (long dashes). The mean emissivity at 53° is plotted (x). The RMS of the angular fit is given for each surface type, along with the RMS error that would be obtained when using a constant emissivity equal to the mean emissivity at 53° (in brackets).

with increasing frequencies from SSM/I measurements at both polarizations. The same trend is confirmed by Xiang and Smith [28] with SSM/I observations of the Sahelian region.

Above 100 GHz, the only satellite emissivity estimates are due to Felde and Pickle [29]. They derive microwave land surface emissivities at 91 and 150 GHz from SSM/T-2 observations collocated with radiosonde measurements, assuming no angular dependence of the surface emissivities. For most land surface types, they estimate an increase in the emissivity between 91 and 150 GHz, although some surface types show the opposite trend.

C. Linear Interpolation/Extrapolation of the SSM/I Emissivities up to 100 GHz

Between 19 and 90 GHz, emissivity changes with frequency are within 0.1 for most land surface types excluding very wet bare soil, snow, and ice. The satellite estimates show a small and slow decrease of the emissivity with increasing frequency, while field experiments usually show an increase of the emissivity

with increasing frequency over bare soil and various frequency behaviors over vegetated areas, depending on the vegetation and observation characteristics. Several factors could explain the different behaviors observed with satellite and field measurements. Because SSM/I observes at a rather large zenith angle (53°), the SSM/I observations are very sensitive to the presence of vegetation even when sparse. Most field measurements over vegetated surfaces show a small frequency dependence of the emissivity that can be positive or negative depending on the vegetation type. The diversity of surface types that have been measured by field experiment is limited. Surface types that are widely spread over the globe-like rain forest or deserts have never been the object of specific observations. The effect of large scale roughness (topography), which cannot be measured by field experiments, could also be responsible for discrepancies between satellite and field observations. This topography effect, combined with the averaging process within a satellite field-of-view, could explain why the low emissivities associated with large frequency changes that characterize field measurements over smooth surfaces are rarely observed from satellites.

Given the small frequency variations of the SSM/I surface emissivities, the most conservative assumption for values at other frequencies is that they can be obtained by linearly interpolating or extrapolating the microwave SSM/I emissivities for the SSM/T and AMSU frequencies up to 100 GHz at least, except for snow and ice areas. In Section V, we will discuss some preliminary results we obtain with SSM/T-2 at 150 GHz.

IV. THE ANGULAR DEPENDENCE OF THE MICROWAVE LAND SURFACE EMISSIVITIES

The SSM/T and AMSU instruments are both cross-track scanners. SSM/T has seven scan positions θ_s from -39° to $+39^\circ$ and SSM/T-2 has 28 positions from -40.5° to $+40.5^\circ$. These are satellite view angles which translate into local zenith angles θ_z up to 47.4° near the edge of the scan due to the curvature of the Earth. AMSU-A has 30 scan positions at 3.3° intervals from $-14.5 \times 3.3^\circ$ to $+14.5 \times 3.3^\circ$, while AMSU-B has 90 positions at 1.1° intervals from $-44.5 \times 1.1^\circ$ to $+44.5 \times 1.1^\circ$, which translate into local zenith angles θ_z up to 58.5° . The polarization measured by SSM/T and AMSU rotates with scan angle due to the rotating-reflector/fixed-feed type of antenna design. If θ_s is the scan angle and θ_z is the local zenith angle, then the SSM/T or AMSU surface emissivity $\epsilon(\theta_z)$ seen for a local zenith angle θ_z is given by

$$\epsilon(\theta_z) = \epsilon_p(\theta_z) \cos^2(\theta_s) + \epsilon_q(\theta_z) \sin^2(\theta_s) \quad (4)$$

$\epsilon_p(\theta_z)$ and $\epsilon_q(\theta_z)$ are the two orthogonal polarized surface emissivities at θ_z local zenith angle. Depending on the channels, p will represent the vertical or the horizontal polarization. The polarization p seen when the incidence is close to nadir (i.e. for $\theta_z = \theta_s$ very close to 0°) is indicated for each channel on Table I. $\theta_s = 45^\circ$ corresponds to $\theta_z = 53^\circ$, which is also the SSM/I zenith angle. For this angle, $\epsilon(53^\circ) = (\epsilon_p(53^\circ) + \epsilon_q(53^\circ))/2$.

The polarization state for SSM/T-2 is sometimes given as "unspecified." In some studies ([29] for instance), SSM/T-2 has been assumed to observe vertical polarization at nadir, whereas

horizontal polarization at nadir has been assumed by Wessel and Boucher [30] in their comparison of the SSM/I and SSM/T-2 window channels near 90 GHz. From comparisons between observations and simulations, Burns *et al.* [31] concluded that the instrument is observing the horizontal polarization at nadir and this has been confirmed to them by information from the Aerojet system engineers for the SSM/T-2 project.

The SSM/I emissivities are only available at one zenith angle (53°) and for two orthogonal polarizations, giving no information on the emissivity angular dependence.

Model results derived from the INRA measurements are analyzed to estimate the angular dependence of the emissivity. The INRA model is used to simulate the surface emissivities at frequencies up to 100 GHz, for angles between 0° and 60° and for two orthogonal polarizations. The results are presented in Fig. 3 at 90 GHz for different surface types (smooth and rough bare soils and a wheat field).

Vegetation induces absorption/emission and scattering of the microwave radiation so that emission is almost unpolarized and insensitive to the angle of incidence. This is fortunate since most surfaces are vegetated, leaving only the necessity for interpolating or extrapolating the frequency dependence of the emissivity (see Section III). For bare soils, the surface emission is polarized and varies with scan angle. From (4), the surface emissivity that would be seen by SSM/T or AMSU is calculated and the result at 90 GHz is shown in Fig. 3 (solid lines) for the case of vertical polarization close to nadir (i.e. $p = V$ and $q = H$ in (4)). Because of the rotation of the polarizations with the scan angle, the surface emissivity varies less with scan angle than the two orthogonal polarizations do separately (this is also true for the case of horizontal polarization close to nadir). However, for bare soils, the angular dependence is still significant.

How can we infer the SSM/T or AMSU emissivity for all the scan angles, knowing only an estimate of the surface emissivity for horizontal and vertical polarizations at 53°? This question has also been raised by Felde and Pickle [29] for SSM/T-2. In their effort to estimate the surface emissivities at 90 and 150 GHz, they simulate the SSM/T-2 emissivity over water surfaces and they conclude that the SSM/T-2 emissivities could be considered fixed with angle. Although this approximation is acceptable for vegetated areas, it is not representative of bare soil surfaces.

For each frequency measured at INRA and for each polarization pattern corresponding to the cross-track scanners [vertical or horizontal at nadir according to (4)], a single polynomial function of the angle, based only on the two orthogonal emissivities at 53°, is tested to best-fit the angular variations of the surface emissivities that would be seen by the cross-track scanning instruments (SSM/T-2 or AMSU), for all the surface types measured at INRA. Several functional forms have been examined and the following one is selected:

$$\begin{aligned} \epsilon(\theta_z) &= F(\epsilon_V(53^\circ), \epsilon_H(53^\circ), \theta_z) \\ &= [\epsilon_V(53^\circ) + \epsilon_H(53^\circ)]/2 \\ &\quad + [\epsilon_V(53^\circ) - \epsilon_H(53^\circ)] \\ &\quad \times (a_0 + a_1\theta_z + a_2\theta_z^2 + a_3\theta_z^3) \end{aligned} \quad (5)$$

TABLE III
ANGULAR MODEL PARAMETERS

Frequency (GHz)	a_0	a_1	a_2	a_3
		<i>V nadir</i>		
23.8	0.13	-5.99e-3	5.21e-4	-0.86e-5
36.5	0.24	-7.56e-3	6.33e-4	-1.09e-5
90.0	0.37	-9.46e-3	7.61e-4	-1.35e-5
f	$3.27e-3 \times f$ +0.08	$-4.74e-5 \times f$ -5.29e-3	$3.26e-6 \times f$ +4.75e-4	$-0.66e-7 \times f$ -0.77e-5
		<i>H nadir</i>		
23.8	0.13	-4.67e-3	-0.07e-4	0.09e-5
36.5	0.24	-6.22e-3	1.04e-4	-0.14e-5
90.0	0.37	-7.61e-3	2.18e-4	-0.40e-5
f	$3.27e-3 \times f$ +0.08	$-3.90e-5 \times f$ -4.21e-3	$3.602e-6 \times f$ -0.46e-4	$-0.66e-7 \times f$ +0.18e-5

where θ_z is the zenith angle expressed in degrees. It corresponds to a Taylor expansion in θ_z around the mean emissivity value at 53°.

For each frequency measured at INRA and for each polarization pattern corresponding to the cross-track scanners, a single set of coefficients a_n is calculated to minimize the RMS errors between the fitted $F(\epsilon_V(53^\circ), \epsilon_H(53^\circ), \theta_z)$ and the simulated emissivities for all the surface types measured at INRA. Fig. 3 shows the AMSU simulated emissivities (solid line) and the fit at 90 GHz for each surface type, along with the RMS error (RMSE) between the fit and the model. The RMSE is ≤ 0.015 , whatever the surface type. The “x” symbol in Fig. 3 indicates the mean of the two orthogonal polarizations at 53°. The RMSE resulting from the use of this mean value regardless of the zenith angle is indicated in brackets. The RMSE given by the angular dependent function is better or comparable to the RMSE obtained with a fixed mean value. The corresponding a_n coefficients are indicated on Table III for 23.8, 36.5 and 90 GHz, for the two possible polarization patterns, i.e. with horizontal or vertical polarizations close to nadir. For each a_n coefficient, a linear regression in frequency is applied, and the corresponding $a_n(f)$ are also presented in Table III as a function of the frequency f . This is equivalent to applying a linear regression to the whole function.

The function in (5) is then tested on different surface types using the RADTRAN model, and the $a_n(f)$ previously calculated. The results are presented in Fig. 4 for two AMSU-A frequencies. For bare soils and for vegetated areas, the function in (5) represents well the model angular dependence, with RMSE lower than 0.015. For open water surfaces, the angular dependence of the surface emissivity is not well reproduced. These surfaces are characterized by low emissivities at 53° for the horizontal polarization (≤ 0.5 at 19 GHz). They represent less than 1% of the surface emissivities as calculated from SSM/I and are concentrated in lake or coast areas. These pixels can be processed separately.

V. VERIFICATION OF THE METHOD FOR SSM/T-2 OBSERVATIONS AT 91.655 GHz AND AT FREQUENCIES ABOVE 100 GHz

From the analysis of the frequency and angular dependences of the microwave surface emissivities (Sections III and IV),

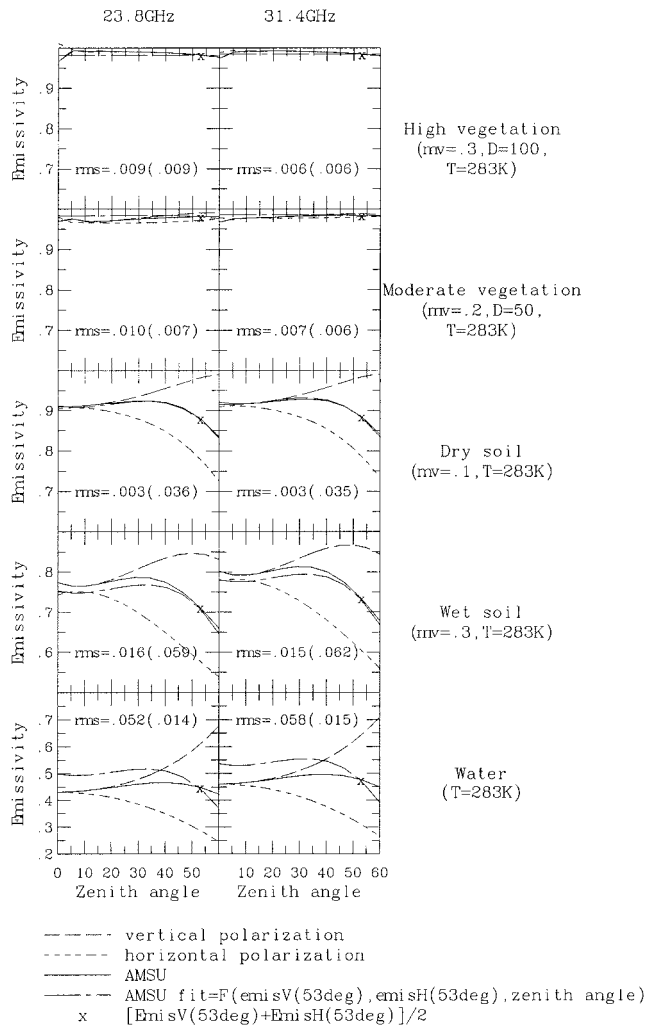


Fig. 4. Surface emissivities simulated with the RADTRAN code for two AMSU frequencies for different surface types. The fitted curves are also shown and the RMS error of the fit is indicated, along with the RMS error that would be obtained when using a constant emissivity equal to the mean emissivity at 53° (in brackets). For bare soils, m_v represents the volumetric moisture content in soil. For vegetation, m_v represents the volumetric moisture content in soil, and D is the depth of the vegetation layer in cm.

SSM/T and AMSU emissivities up to 100 GHz can be estimated from SSM/I emissivities. First, the SSM/I emissivities measured at 53° for vertical and horizontal polarizations are linearly interpolated or extrapolated in frequency for the SSM/T or AMSU frequency of interest f for each polarization. It gives the $\epsilon_H(53^\circ)$ and $\epsilon_V(53^\circ)$ for frequency f . Then (5) is applied to the frequency interpolated emissivities $\epsilon_V(53^\circ)$ and $\epsilon_H(53^\circ)$. The coefficients to be used in (5) are calculated from Table III for the AMSU or SSM/T frequency f .

We first verify this method against SSM/T observations at 91.655 GHz, and then we examine a possible extension of the method above 100 GHz.

A. SSM/T-2 Observations at 91.655 GHz

With the same method applied to SSM/I, using NCEP and ISCCP ancillary data, the land surface emissivities are estimated at 91.655 and 150 GHz directly from SSM/T-2 observations as

a function of zenith angles up to 47.4° . For the F-11 DMSP satellite, scan positions above 24 (i.e., scan angles larger than 18.5° in one side of the scan) have been filtered out because of an instrument problem (interference with the glare obstructor) [32]. The 150 GHz channel failed on the F-11 but data are available from the F-12 satellite. Fig. 5 presents the emissivity maps at 91.655 GHz for three different zenith angles (1.7° , 25.7° , and 47.4°) for April 1994. Because SSM/T-2 is a cross-track scanner, each location on the Earth is not seen with the same zenith angle very often. For most pixels, the monthly mean emissivities presented on Fig. 5 are based on only one value, which limits the reliability of these estimates.

The monthly mean land surface emissivities are calculated from SSM/I for April 1993 for the nominal 53° zenith angle (note different year than SSM/T-2 data). To test our method, the SSM/I emissivities at 85.5 GHz are first linearly extrapolated up to 91.655 GHz. The angular fit derived from the INRA model [(5) and Table III] is applied to these extrapolated emissivities and the results are presented in Fig. 5 for the same three zenith angles. The SSM/I derived emissivities are given on a 0.25° grid while the SSM/T-2 calculations could only be performed on a 0.33° grid because of the lower spatial instrument resolution. For most locations, more than ten values are available from SSM/I to derive a monthly mean [16]. For all zenith angles, the spatial variability of the SSM/T-2 emissivities is well captured by the SSM/I derived emissivities. Large differences are concentrated along the coast and in Eastern Europe (these areas have been excluded from the statistics presented on Fig. 5). The large differences along the coast are related to the different spatial resolutions of the instruments producing different mixes of land and water. In Eastern Europe, the variability in snow cover between April 1993 and April 1994 is responsible for the change in surface emissivities. For comparison purposes, the SSM/I derived emissivities are averaged over the SSM/T-2 fields-of-view, taking into account the increasing fields-of-view of the SSM/T-2 instrument with increasing zenith angle. The cross-correlation coefficients between the SSM/T-2 and the SSM/I-derived emissivities are ≈ 0.8 for all zenith angles. The histograms of the differences between the SSM/T-2 emissivities at 91.655 GHz and the SSM/I derived emissivities are presented on Fig. 5 for three zenith angles. The results obtained when using a mean emissivity calculated at 53° , regardless of the zenith angle, are also shown with dashed lines. When using the angle-dependent model, the mean error (< 0.01) and the RMS (≈ 0.02) are similar or lower for all scanning angles than when using the mean emissivity. Note that more than half the RMS differences in Fig. 5 can be accounted for by the intrinsic variations in the SSM/I emissivity values. This variability appears in a single month and can be expected to appear year-to-year [16].

B. Possible Extension of the Method to Frequencies Above 100 GHz

Fig. 6 presents the 150 GHz emissivities for February 1995 for three zenith angles, along with the emissivity difference between 150 and 91.655 GHz. For desert and sparse vegetation, the emissivities at 150 GHz are lower than at 91.655 GHz. This

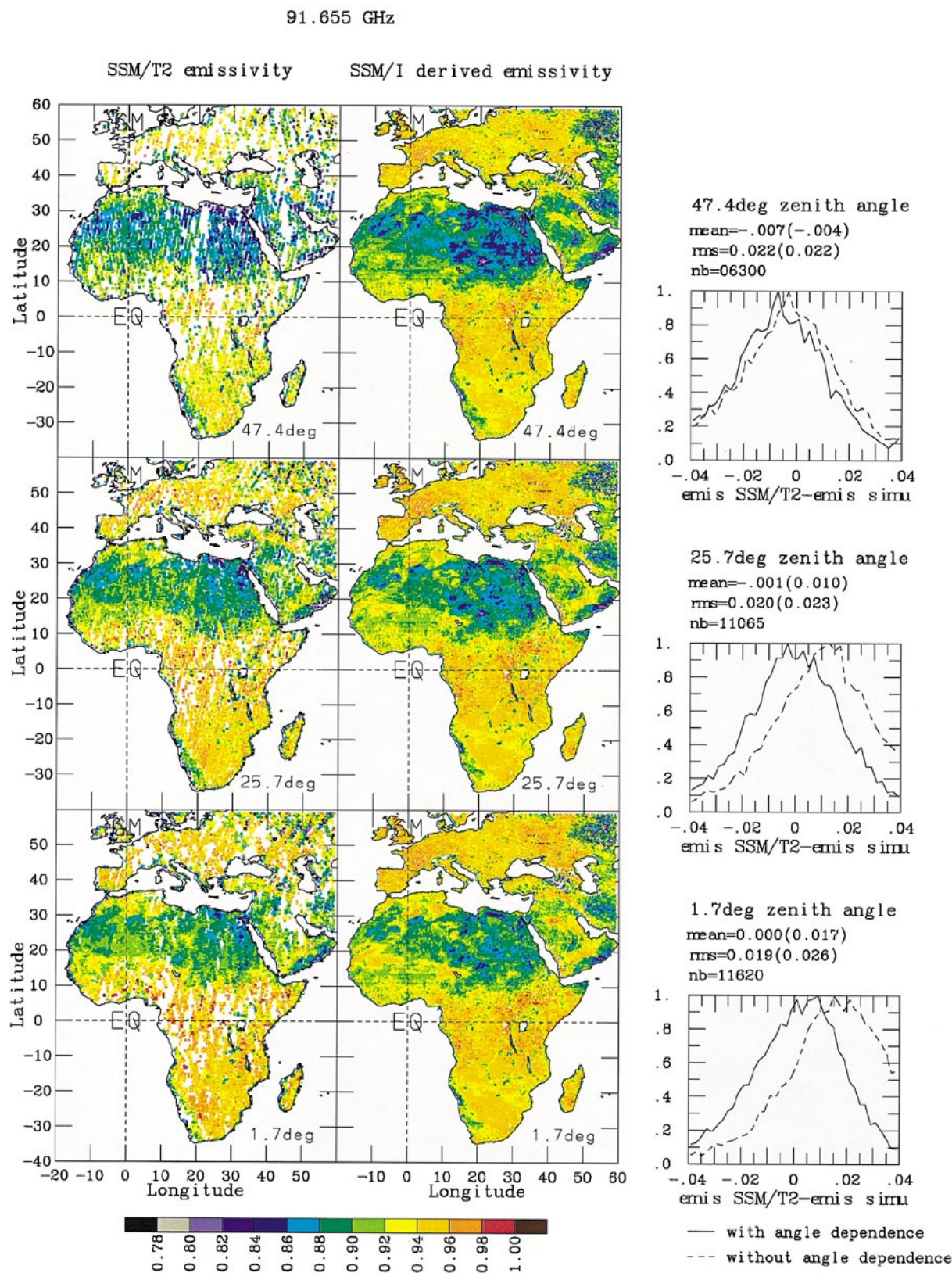


Fig. 5. Emissivity maps at 91.655 GHz at 1.7°, 25.7°, and 47.4° zenith angle, as calculated from SSM/T-2 and as derived from SSM/I estimations. The histograms of the difference are presented for the three angles (solid line) along with the mean and RMS errors and the number of pixels considered in the calculation (nb). The histograms of the difference when considering the mean SSM/I emissivity at 53° is also indicated (dashed line), with the mean and RMS errors in brackets.

is not always the case for densely vegetated areas. These results are consistent with Felde and Pickle [29], who also found dif-

ferent spectral variations depending on the surface type. However, as previously mentioned, Hewison [15] found higher emis-

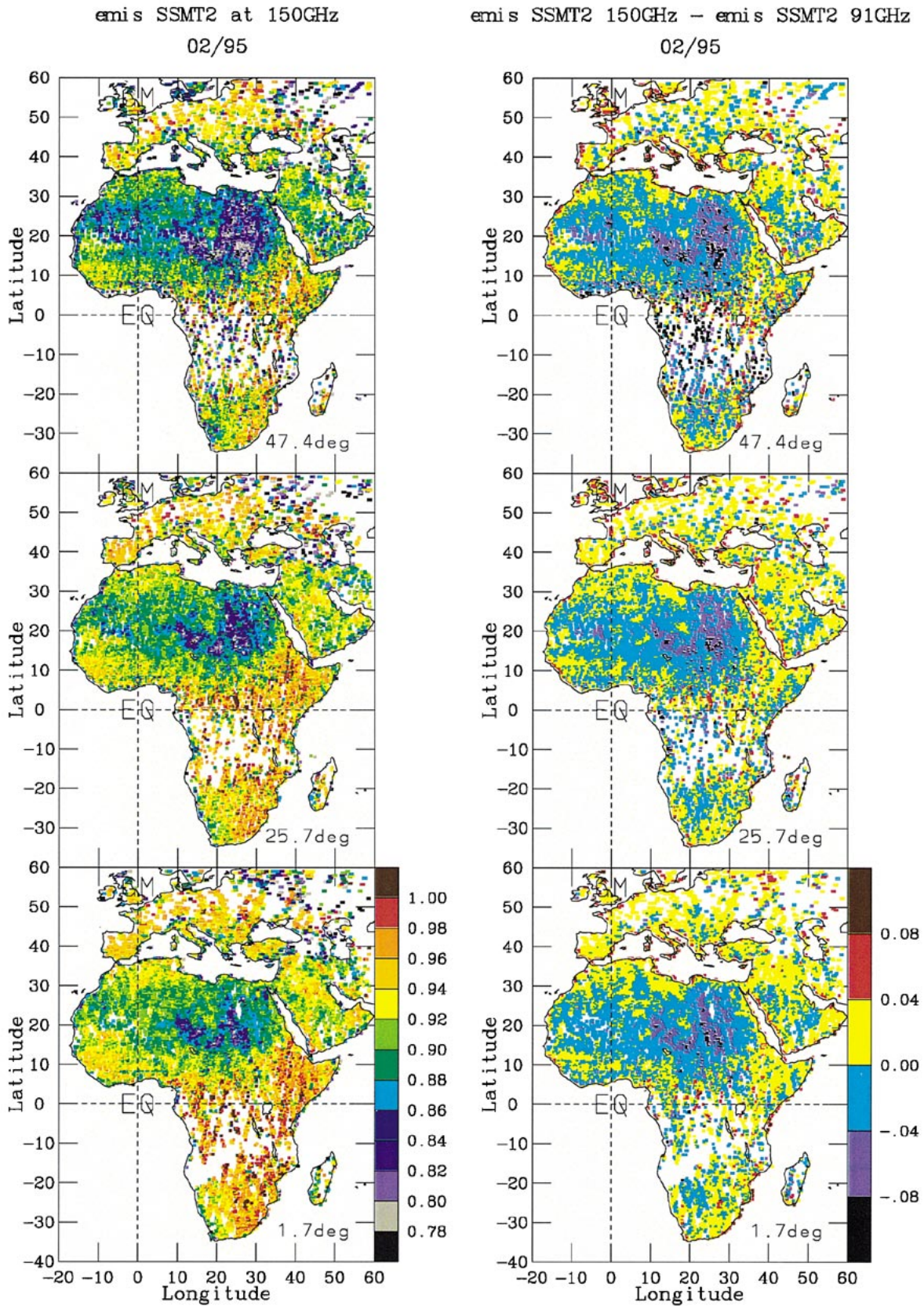


Fig. 6. Emissivity maps at 150 GHz at 1.7°, 25.7°, and 47.4° zenith angle, as calculated from SSM/T-2 for February 1995, along with the difference between the emissivities at 150 GHz and the emissivities at 91.655 GHz.

sivity at 150 GHz than at 89 GHz at nadir for all the surfaces he observed. Several 5° × 5° areas, where the surface types are sup-

posed to be homogeneous, have been selected to illustrate the angular dependence of the surface emissivities at 91.655 and

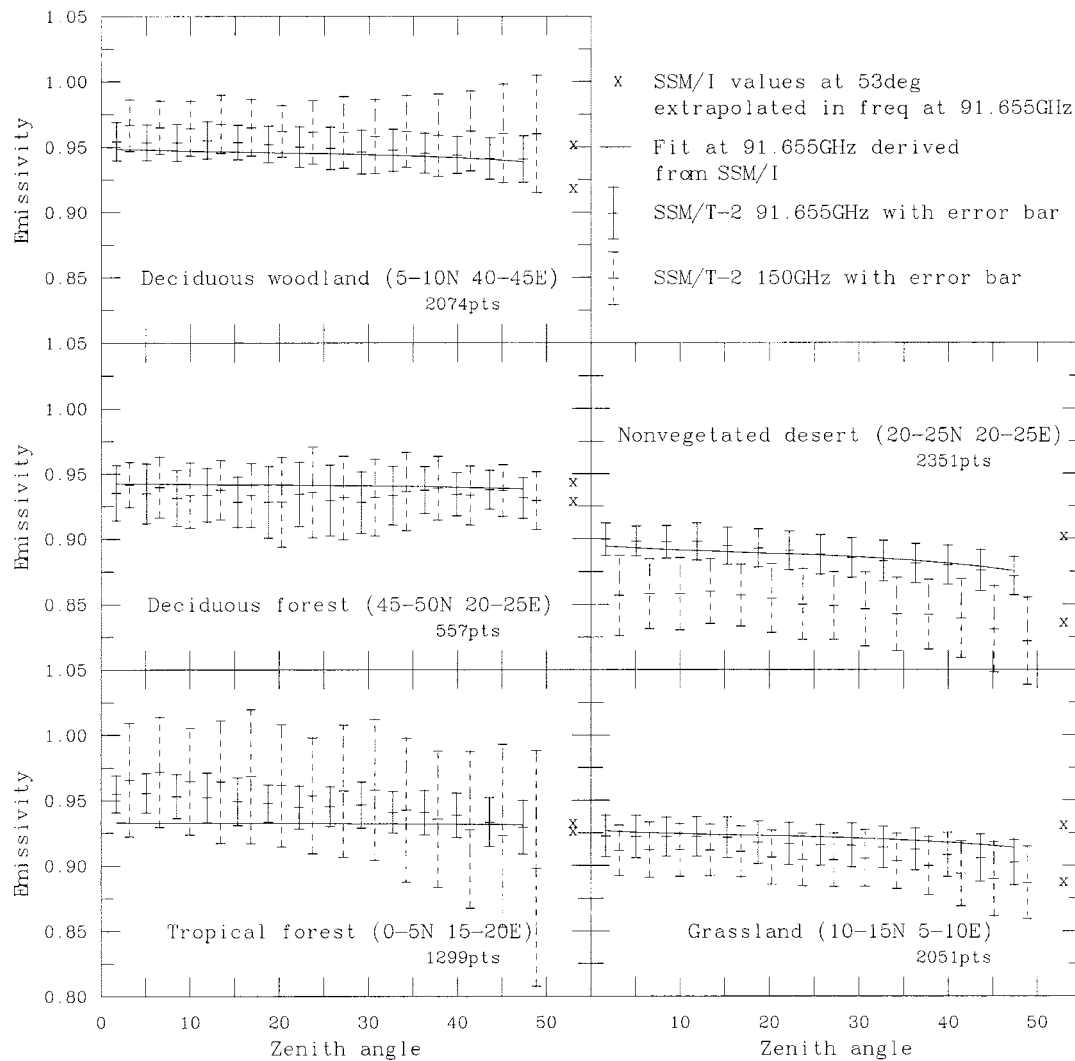


Fig. 7. Angular dependence of the emissivities at 91.655 and 150 GHz for five surface types, as observed with SSM/T-2. The mean values and the standard deviations are presented for each $5^\circ \times 5^\circ$ area. The corresponding SSM/I emissivity values extrapolated in frequencies at 91.655 GHz (x) are added to the figures for both vertical and horizontal polarizations. The angular fit at 91.655 GHz is computed from those values and the result is drawn (solid line).

150 GHz, as estimated from SSM/T-2 measurements (Fig. 7). For each zenith angle, the mean value is indicated along with the associated standard deviation. As expected, at 91.655 GHz, the angular dependence for bare soil and sparse vegetation is stronger than for densely vegetated areas. Despite a large scatter in the results, it appears that the angular dependence of the emissivities over tropical forest is stronger at 150 GHz than at 91 GHz. Over deciduous forests, Hewison [15] also measured a larger than expected angular dependence at 150 GHz. At 150 GHz, the standard deviations of the results are larger especially in tropical areas for large zenith angles. This is probably related to the larger atmospheric contribution at this frequency, especially in tropical areas.

Fig. 8 shows the change in the estimated emissivity for a given change in the atmospheric contribution (increase in the water vapor continuum absorption or increase in the water vapor column abundance) at 91 and 150 GHz for three standard atmospheres. The emissivity estimations are not very sensitive to changes in the atmospheric water vapor contribution, except

in tropical regions at 150 GHz and especially for zenith angles above 20° . To explain the observed large angular trend over the tropical forests in terms of error in the water vapor continuum absorption at 150 GHz, it would have to be increased by close to 20% (see Fig. 8), which is not realistic. The results presented in this paper at 150 GHz have been obtained using the MPM 89 gaseous absorption model [33]. This model has been shown to slightly underestimate the water vapor absorption at 150 GHz for tropical atmospheres [34], and Rosenkranz [35] proposed a correction to this model. We have recalculated the emissivities using this new model and the results are not very different. There is still a large angular dependence of the surface emissivities at 150 GHz over tropical forest.

At this point, it appears that a simple frequency extrapolation from 90 to 150 GHz will not give satisfactory results. The scarcity of emissivity field measurements, the lack of validated models, and the few satellite estimations available will not help fill the gap. Before reaching any conclusion, longer time series of satellite data at 150 GHz will have to be processed,

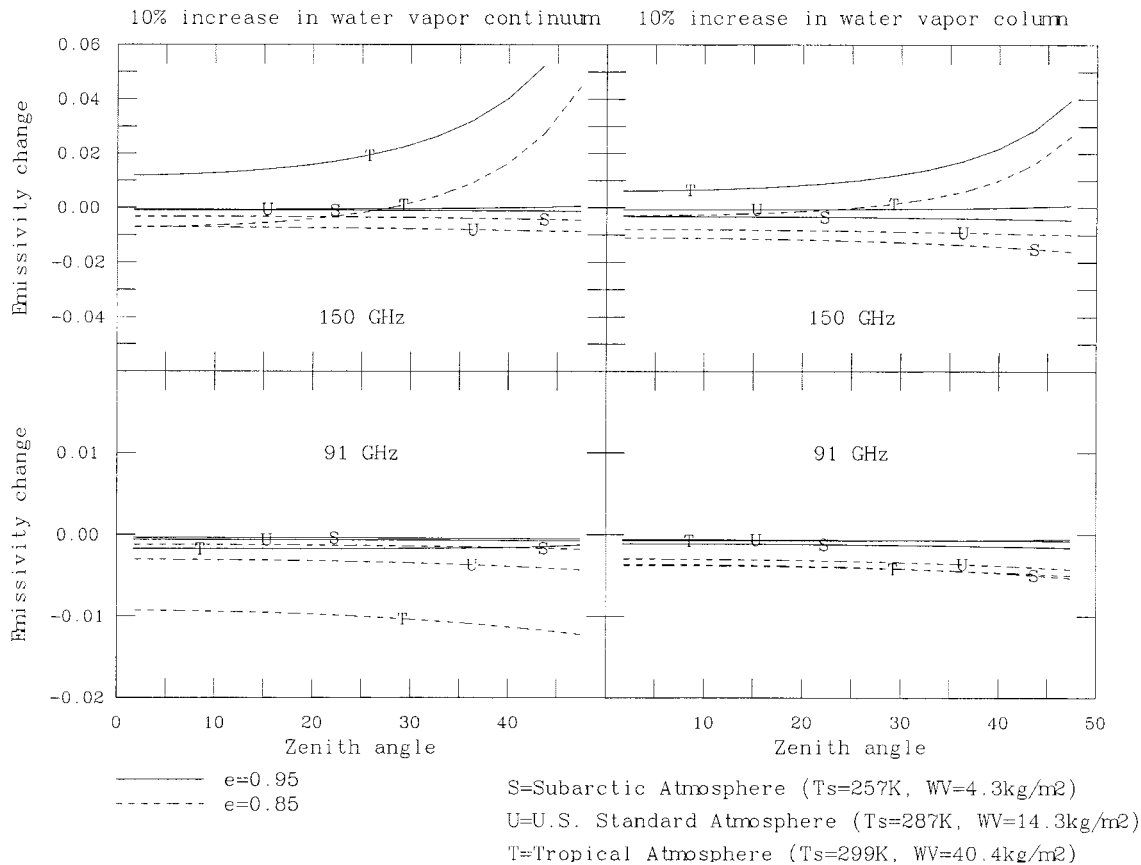


Fig. 8. Sensitivity of the estimated emissivities to changes in the water vapor column or continuum absorption model at 91 and 150 GHz for three standard atmospheres and for two initial land surface emissivities.

and because of the sensitivity of this frequency to water vapor absorption, special attention will have to be paid to both the water vapor profile estimation and the water vapor absorption model. These estimations may have to be performed in the context of a simultaneous retrieval of atmospheric and surface parameters.

VI. CONCLUSION

The land surface emissivities have been previously calculated for the globe from the SSM/I conical scanner at 19, 22, 35, 85 GHz for vertical and horizontal polarizations (except for 22 GHz, which is vertical only) at 53° zenith angle. The SSM/T and AMSU temperature and humidity sounders are cross-track scanners, and they both have channels that are sensitive to the surface. To analyze the feasibility of deriving SSM/T and AMSU land surface emissivities from SSM/I emissivities, the spectral and angular variations of land surface emissivities are studied with the help of ground-based emissivity measurements, emissivity models, and satellite emissivity estimates.

Up to 100 GHz for snow and ice-free areas, the SSM/T and AMSU emissivities can be derived with useful accuracy from the SSM/I emissivities. For a given zenith angle, the emissivities can be linearly interpolated in frequency. The scanning and polarization patterns of SSM/T and AMSU are such that the angular dependence of the emissivity seen by

these instruments is rather small. Based on ground-based emissivity measurements of various surface types, a simple model is proposed to estimate SSM/T and AMSU emissivities for all zenith angles knowing only the emissivities for the vertical and horizontal polarizations at 53° zenith angle. The method is tested on the SSM/T-2 91.655 GHz channel. The spatial variability of the surface emissivities is well captured. The mean difference between the SSM/T-2 emissivities and the SSM/I-derived emissivities at 91.655 GHz is lower than 0.01 for all zenith angles with an RMS difference of ~ 0.02 . An atlas of the SSM/I land surface emissivities is available with a 0.25° resolution. The inter- and intra-annual variability of the emissivities is now under study. With the method developed in this paper, emissivity maps at AMSU-A frequencies and scanning conditions are being prepared for the French Meteorological Office, Centre de Meteorologie Spatiale, Lannion, France. They will be used as emissivity first guesses in the temperature profile retrieval scheme.

Above 100 GHz, preliminary results have been presented at 150 GHz based on SSM/T-2 observations. These results are compared with the very few estimations available in the literature. It appears that a simple frequency extrapolation from 90 GHz to 150 GHz will not give satisfactory results. Longer time series of satellite data at 150 GHz will have to be processed, and because of the sensitivity of this frequency to water vapor absorption, special attention will have to be

paid to both the water vapor profile estimation and the water vapor absorption model.

ACKNOWLEDGMENT

The authors wish to thank M. Rothstein, NASA/GISS, New York, for his help in processing the satellite data sets and Dr. J. Bates, NOAA/ERL, Boulder, CO, for providing the SSM/T-2 data. They would also like to thank three anonymous reviewers for their comments and suggestions. NCAR/NCEP reanalysis data have been provided through the NOAA Climate Diagnostics Center (<http://www.cdc.noaa.gov>).

REFERENCES

- [1] H. E. Fleming, N. C. Grody, and E. J. Kratz, "The forward problem and corrections for the SSM/T satellite microwave temperature sounder," *IEEE Trans. Geosci. Remote Sensing*, vol. 29, pp. 571–584, July 1991.
- [2] V. J. Falcone, M. K. Griffin, R. G. Isaacs, J. D. Pickle, J. F. Morrissey, A. J. Jackson, A. Bussey, R. Kakar, J. Wang, P. Racette, D. J. Boucher, B. H. Thomas, and A. M. Kishi, "SSM/T-2 Calibration and Validation Data Analysis," Phillips Lab., Hanscom Air Force Base, MA, Tech. Rep. 92-2293, 1992.
- [3] G. R. Diak, D. Kim, M. S. Whipple, and X. Wu, "Preparing for the AMSU," *Bull. Amer. Meteorol. Soc.*, vol. 73, pp. 1971–1984, 1992.
- [4] R. W. Saunders, "Note on the advanced microwave sounding unit," *Bull. Amer. Meteorol. Soc.*, vol. 74, pp. 2211–2212, 1993.
- [5] S. English, "Estimation of temperature and humidity profile information from microwave radiances over different surface types," *J. Appl. Meteorol.*, vol. 38, pp. 1526–1541, 1999.
- [6] A. Guissard and P. Sobieski, "An approximate model for the microwave brightness temperature of the sea," *Int. J. Remote Sensing*, vol. 8, pp. 1607–1627, 1987.
- [7] P. W. Rosenkranz, "Rough-sea microwave emissivities measured with the SSM/I," *IEEE Trans. Geosci. Remote Sensing*, vol. 30, pp. 1081–1085, Sept. 1992.
- [8] C. Guillou, S. J. English, C. Prigent, and D. C. Jones, "Passive microwave airborne measurements of the sea surface response at 89 and 157 GHz," *J. Geophys. Res.*, vol. 101, pp. 3775–3788, 1996.
- [9] C. Matzler, "Seasonal evolution of microwave radiation from an oat field," *Remote Sens. Environ.*, vol. 31, pp. 161–173, 1990.
- [10] J.-P. Wigneron, A. Chanzy, J.-C. Calvet, and N. Bruguier, "A simple algorithm to retrieve soil moisture and vegetation biomass using passive microwave measurements over crop fields," *Remote Sens. Environ.*, vol. 51, pp. 331–341, 1995.
- [11] A. Chanzy, S. Raju, and J.-P. Wigneron, "Estimation of soil microwave effective temperature at L and C bands," *IEEE Trans. Geosci. Remote Sensing*, vol. 35, pp. 570–580, May 1997.
- [12] J.-C. Calvet, A. Chanzy, and J.-P. Wigneron, "Surface temperature and soil moisture retrieval in the Sahel from airborne multifrequency microwave radiometry," *IEEE Trans. Geosci. Remote Sensing*, vol. 34, pp. 588–600, 1996.
- [13] J.-P. Wigneron, D. Guyon, J.-C. Calvet, G. Courrier, and N. Bruguier, "Monitoring coniferous forest characteristics using a multifrequency (5–90 GHz) microwave radiometer," *Remote Sens. Environ.*, vol. 60, pp. 299–310, 1997.
- [14] T. J. Hewison and S. J. English, "Airborne retrievals of snow and ice surface emissivity at millimeter wavelength," *IEEE Trans. Geosci. Remote Sensing*, vol. 37, pp. 1871–1879, July 1999.
- [15] T. J. Hewison, "Airborne measurements of land surface emissivity at millimeter wavelength," *IEEE Trans. Geosci. Remote Sensing*, to be published.
- [16] C. Prigent, W. B. Rossow, and E. Matthews, "Microwave land surface emissivities estimated from SSM/I observations," *J. Geophys. Res.*, vol. 102, pp. 21 867–21 890, 1997.
- [17] —, "Global maps of microwave land surface emissivities: Potential for land surface characterization," *Radio Sci.*, vol. 33, pp. 745–751, 1998.
- [18] J. P. Hollinger, R. Lo, G. Poe, R. Savage, and J. Pierce, "Special Sensor Microwave/Imager User's Guide," Nav. Res. Lab., Washington, D.C., 1987.

- [19] W. B. Rossow, A. W. Walker, D. E. Beuschel, and M. D. Roiter, "International Satellite Cloud Climatology Project (ISCCP): Document on New Cloud Datasets," Nat. Aeronaut. Space Admin., Goddard Inst. Space Studies, New York, 1996.
- [20] E. Kalnay *et al.*, "The NCEP/NCAR 40-year reanalysis project," *Bull. Amer. Meteorol. Soc.*, vol. 77, pp. 437–470, 1996.
- [21] J. R. Wang and B. J. Choudhury, "Remote sensing of soil moisture content over bare field at 1.4 GHz frequency," *J. Geophys. Res.*, vol. 86, pp. 5277–5282, 1981.
- [22] J.-C. Calvet, J.-P. Wigneron, A. Chanzy, S. Raju, and L. Laguerre, "Microwave dielectric properties of a silt-loam at high frequencies," *IEEE Trans. Geosci. Remote Sensing*, vol. 33, pp. 634–642, 1995.
- [23] C. Matzler, "Passive microwave signatures of landscapes in winter," *Meteorol. Atmos. Phys.*, vol. 54, pp. 241–260, 1994.
- [24] R. G. Isaacs, Y.-Q. Jin, R. D. Worsham, G. Deblonde, and V. J. Falcone, "The RADTRAN microwave surface emission models," *IEEE Trans. Geosci. Remote Sensing*, vol. 27, pp. 433–440, 1989.
- [25] E. Matthews, "Global vegetation and land use: New high-resolution data bases for climate studies," *J. Clim. Appl. Meteorol.*, vol. 22, pp. 474–486, 1983.
- [26] B. J. Choudhury, "Reflectivities of selected land surface types at 19 and 37 GHz from SSM/I observations," *Remote Sens. Environ.*, vol. 46, pp. 1–17, 1993.
- [27] A. S. Jones and T. H. Vonder Haar, "Retrieval of surface emittance over land using coincident microwave and infrared satellite measurements," *J. Geophys. Res.*, vol. 102, pp. 13 609–13 626, 1997.
- [28] X. Xiang and E. A. Smith, "Feasibility of simultaneous surface temperature-emissivity retrieval using SSM/I measurements from HAPEX-Sahel," *J. Hydrol.*, vol. 188–189, pp. 330–360, 1997.
- [29] G. W. Felde and J. D. Pickle, "Retrieval of 91 and 150 GHz Earth surface emissivities," *J. Geophys. Res.*, vol. 100, pp. 20 855–20 866, 1995.
- [30] J. E. Wessel and D. Boucher, "Comparison between cross-track and conical scanning microwave window channels near 90 GHz," *IEEE Trans. Geosci. Remote Sensing*, vol. 36, pp. 16–24, Jan. 1998.
- [31] B. Burns, X. Wu, and G. R. Diak, "Impact of emissivity model errors on retrieval of water vapor profiles over ocean with SSM/T2," in *Int. Geoscience and Remote Sensing Symp. '98*, Seattle, WA, 1998.
- [32] T. J. Kleespies, "Some anomalies in the SSM/T-2 antenna temperatures," in *8th Conf. Satellite Meteorology and Oceanography*, 1996, pp. 134–136.
- [33] H. J. Liebe, "MPM—An atmospheric millimeter-wave propagation model," *Int. J. Inf. Millim. Waves*, vol. 10, pp. 631–650, 1989.
- [34] S. J. English, C. Guillou, C. Prigent, and P. J. Jones, "Aircraft measurements of water vapour continuum absorption at millimetre wavelength," *Q. J. R. Meteorol. Soc.*, vol. 120, pp. 603–625, 1994.
- [35] P. W. Rosenkranz, "Water vapor microwave continuum absorption: A comparison of measurements and models," *Radio Sci.*, vol. 33, 1998.

Catherine Prigent received the Ph.D. degree in physics from Paris University, Paris, France, in 1988.

She is a Research Scientist with the Paris Observatory, Centre National de la Recherche Scientifique (CNRS), Paris. Since 1995, she has been on leave from the CNRS and she works at NASA Goddard Institute for Space Studies, Columbia University, New York. Her early work focused on modeling of the sea surface emissivities at microwave wavelength and the estimation of atmospheric parameters over ocean from microwave measurements. At present, her main research interests include calculation and analysis of microwave land surface emissivities and estimation of atmospheric and surface parameters over land from microwave satellite observations.

Jean-Pierre Wigneron (M'98) received the engineering degree from SupAero, Toulouse, France, and the Ph.D. degree from the University of Toulouse, Toulouse, France, in 1993.

He is currently a Research Scientist with the Institut National de la Recherche Agronomique (INRA), Avignon, France. His research interests include microwave remote sensing of land surface fluxes and development of retrieval methods. He coordinated the Science Group "Physics of Measurements (Land)" of the SMOS mission. He was Co-Investigator of several ground and airborne international campaigns in the field of microwave radiometry (PORTOS, RESEDA, SMOS).

William B. Rossow received the B.A. degree in physics and mathematics from Hanover College, Hanover, NH, and the M.S. degree in physics and the Ph.D. in astronomy from Cornell University, Ithaca, NY.

He is currently a Physical Scientist with NASA Goddard Institute for Space Studies, Columbia University, New York. His research interests include cloud physics and dynamics, atmospheric radiative transfer, atmospheric dynamics, and satellite remote sensing of the Earth's climate and other planetary atmospheres, about which he has published over 100 papers. His early work focused on the clouds and dynamics of the atmospheres of Venus and Jupiter and he served on the Science Teams for the Pioneer Venus and Galileo (to Jupiter) space missions. His later work has focused on clouds, radiation, and the climate of Earth, as Head of the Earth Observations Group, NASA GISS, and as Head of the Global Processing Center International Satellite Cloud Climatology Project (ISCCP) since 1983. He is a Member of the Science Teams for the Earth Observing System (EOS) spacecraft missions, the Tropical Rainfall Measurement Mission (TRMM), the CloudSat spacecraft mission, the Atmospheric Radiation Measurement (ARM) project, the ScaRab project, and the First ISCCP Regional Experimental (FIRE).

Dr. Rossow serves on several national and international committees, panels, and working groups. He received the NASA Exceptional Scientific Achievement Medal in 1988 and is a Fellow of the American Geophysical Union.



Juan R. Pardo-Carrion received the M.S. degree in physics from Madrid University, Madrid, Spain, in 1992 and the Ph.D. degree in physics from Paris University, Paris, France, in 1996.

He was a Postdoctoral Researcher with NASA/Goddard Institute for Space Studies, Columbia University, New York, from 1997 to 1998, is now with the California Institute of Technology, Pasadena. He developed a radiative transfer model currently used by many millimeter and submillimeter wave telescopes to evaluate atmospheric transmission. Validation of this model is undertaken with a series of observational experiments using a Fourier transform spectrometer installed at Mauna Kea, HI. In addition, he conducts observations with different telescopes to study the physical and chemical conditions of galactic molecular clouds and circumstellar envelopes.